Supplemental information for: Nature of symmetry breaking at the excitonic insulator transition: Ta_2NiSe_5

Giacomo Mazza,[1,2,3,*] Malte Rösner,[4,*] Lukas Windgätter,[5] Simone Latini,[5] Hannes Hübener,[5] Andrew J. Millis,[6,7] Angel Rubio,[5,6,8] and Antoine Georges[3,6,2,9,†]

[1] *Department of Quantum Matter Physics, University of Geneva, Quai Ernest-Ansermet 24, 1211 Geneva, Switzerland*

[2] *CPHT, CNRS, Ecole Polytechnique, IP Paris, F-91128 Palaiseau, France*

[3] *Collège de France, 11 place Marcelin Berthelot, 75005 Paris, France*

[4] *Radboud University, Institute for Molecules and Materials, Heijendaalseweg 135, 6525 AJ Nijmegen, Netherlands*

[5] *Max Planck Institute for the Structure and Dynamics of Matter, Luruper Chaussee 149, 22761 Hamburg, Germany*

[6] *Center for Computational Quantum Physics, Flatiron Institute, New York, NY 10010 USA*

[7] *Department of Physics, Columbia University, New York, NY, 10027 USA*

[8] *Nano-Bio Spectroscopy Group, Departamento de Física de Materiales, Universidad del País Vasco, 20018 San Sebastian, Spain*

[9] *DQMP, Université de Genève, 24 quai Ernest Ansermet, CH-1211 Genève, Suisse*

I. AB-INITIO CALCULATIONS

Our ab-initio calculations are performed using density functional theory (DFT) initially applying the generalized gradient approximation (GGA / PBE)[1] within the PAW formalism[2] as implemented in the Vienna Ab initio Simulation Package (VASP)[3,4]. We start with fully relaxing the internal atomic coordinates of an orthorhombic unit cell with $a \approx 3.51$ Å, $b \approx 14.07$ Å, and $c \approx 15.79$ Å as lattice constants in reasonable agreement with experimental value[5]. To this end we use a $12 \times 12 \times 3$ K-grid and an energy cut-off of 368 eV. The positions are optimized until all forces are smaller than 0.005 eV/ Å.

Due to the layered structure, screening is reduced so that enhanced Coulomb interactions are expected. To take the resulting correlation effects into account, we use the modified Becke-Johnson exchange potential[6], which has been shown to have a similar accuracy as hybrid functional or GW approaches[7]. The involved c_{mbj} parameter is self-consistently find to be $c_{\mathrm{mbj}} = 1.26$ on a $20 \times 20 \times 5$ K-grid.

The resulting Kohn-Sham states are subsequently projected onto six d_{xz}-like Wannier orbitals centered at the Ta and Ni sites, which are maximally localized using the Wannier90 package[8] applying an inner (frozen) window of about ± 0.3 eV around the Fermi level. Thereby, the overlap between the original Kohn-Sham states and the reconstructed ones is maximized throughout the low-energy window.

These six maximally localized Wannier functions are also used as the basis for the evaluation of the Coulomb matrix elements calculated within the constrained Random Phase Approximation (cRPA)[9] as recently implemented by M. Kaltak within VASP[10]. We use in total 120 bands (about 50 unoccupied) and apply the weighted disentanglement procedure from Ref. 11.

II. STRUCTURAL PHASE TRANSITION

Starting from the relaxed orthorhombic geometry we introduce a small distortion to $\beta = 90° + \delta$ (see figure 1) to seed the monoclinic phase and perform a full relaxation allowing for an optimization of the cell shape, cell-volume and atomic coordinates afterwards. To this end we use a $24 \times 16 \times 8$ K-grid and the PBE (GGA) functional. As a result we find distorted angles of α =90.013°, β =90.571° and γ =89.919°, yielding a triclinic structure (changes to the lattice constants are negligible). This corresponds to an in-plane monoclinic distortion combined with a tilting in the direction perpendicular to the planes. While the inter-layer geometry might suffer from neglected van-der-Waals forces, the in-plane structure is mostly governed by electron-lattice couplings which are sufficiently well captured by DFT. The in-plane monoclinic distortion is thus reliable and intrinsically driven already on the level of DFT.

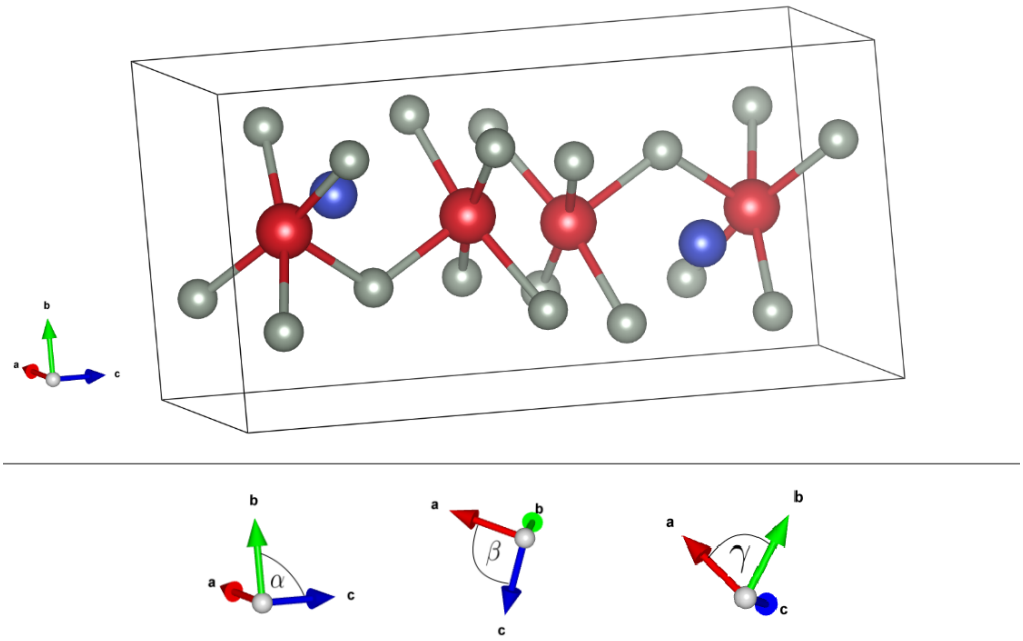

Figure 1. Orthorhombic unit cell. The Tantalum atoms are depicted in red, the Nickel atoms in blue and the Selenium atoms in grey. In the lower part the three angles of the cell are displayed

III. MINIMAL MODEL

We consider a two-dimensional minimal model with six atoms per unit cell (with one d_{xz}-like orbital each) reproducing the double chain structure of a Ta_2NiSe_5 layer. We take into account *i*) single particle hoppings, *ii*) intra-atomic density-density interactions, and *iii*) nearest-neighbor density-density interactions. For simplicity we recall here the definition of the Hamiltonian which we already introduced in the main text:

$$\begin{aligned}\hat{\mathcal{H}} =&\hat{H}_{hop} + \hat{H}_U + \hat{H}_V \\ =&\sum_{\vec{R}\sigma}\sum_{\vec{\delta}} \Psi^\dagger_{\vec{R}+\vec{\delta}}\mathbf{T}(\vec{\delta})\Psi_{\vec{R}\sigma} + U\sum_{\vec{R}}\sum_{j=1,\dots,6}\hat{n}_{j\uparrow}(\vec{R})\hat{n}_{j\downarrow}(\vec{R}) + \\ &+ V\sum_{j=1,2}\sum_{\vec{R}\sigma\sigma'}\left[\hat{n}_{j\sigma}(\vec{R}) + \hat{n}_{j\sigma}(\vec{R}+\vec{\delta}_x)\right]\hat{n}_{5\sigma'}(\vec{R}) + V\sum_{j=3,4}\sum_{\vec{R}\sigma\sigma'}\left[\hat{n}_{j\sigma}(\vec{R}) + \hat{n}_{j\sigma}(\vec{R}-\vec{\delta}_x)\right]\hat{n}_{6\sigma'}(\vec{R}),\end{aligned} \tag{1}$$

with $\Psi_{\vec{R}\sigma}$ a spinor defined as $\Psi^\dagger_{\vec{R}\sigma} \equiv \left(c^\dagger_{1\sigma}(\vec{R})\ c^\dagger_{2\sigma}(\vec{R})\ c^\dagger_{5\sigma}(\vec{R})\ c^\dagger_{3\sigma}(\vec{R})\ c^\dagger_{4\sigma}(\vec{R})\ c^\dagger_{6\sigma}(\vec{R})\right)$ and $\hat{n}_{i\sigma}(\vec{R}) = c^\dagger_{i\sigma}(\vec{R})c_{i\sigma}(\vec{R})$. The hopping matrix $\mathbf{T}(\vec{\delta})$ contains intra-cell $[\mathbf{T}(\vec{0})]$ as well as nearest-cells terms $[\mathbf{T}(\pm a_x, \pm a_y)]$ corresponding to the main contributions of the Wannier Hamiltonian derived above. These matrix elements are summarized in the scheme of Fig. 2(A), which includes Ta-Ta (a) and Ni-Ni (b) intra-chain, Ta-Ni intra- (c)-(d) and inter-chain (e)-(f) hoppings as well as inter-chain Ni-Ni (g) and Ta-Ta (j)-(h) hoppings. Dashed/full pairs of arrows indicate that in order to preserve the symmetry, these matrix elements must be anti-symmetric under a reflection with respect to a plane perpendicular to the chains. We have also indicated symmetry-forbidden Ta-Ni hybridization, that become non-zero upon symmetry breaking. The matrix elements are summarized in the Table I. Fig. 2(B) shows the comparison between the band structure of the minimal and the Wannier model.

A. Hartree-Fock

We consider a single-particle variational wavefunction $|\Psi_0\rangle$ that allows for the breaking of the crystal symmetries. The variational energy is computed by decoupling the interaction terms in the standard way:

$$\langle\Psi_0|\hat{n}_{j\uparrow}(\vec{R})\hat{n}_{j\downarrow}(\vec{R})|\Psi_0\rangle \approx \langle\Psi_0|\hat{n}_{j\uparrow}(\vec{R})|\Psi_0\rangle\langle\Psi_0|\hat{n}_{j\downarrow}(\vec{R})|\Psi_0\rangle \tag{2}$$

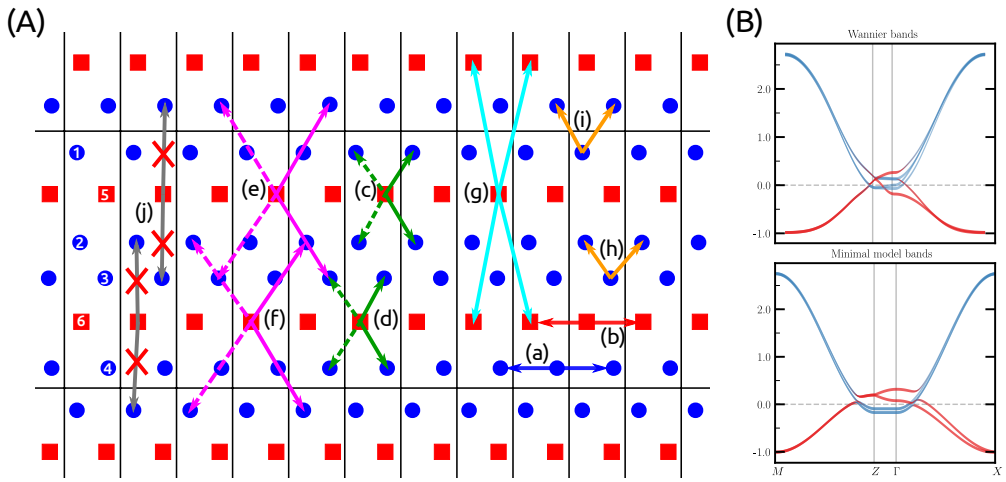

Figure 2. (A) Hopping processes defining the minimal model. Letters are used to group different hopping processes according to the table I. (B) Comparison between the Wannier (top) and the minimal model (bottom) band structure.

Hopping matrix elements $\mathbf{T}(\vec{\delta})$	
Intra-chain Ta-Ta hopping (a)-(b)	$T_{ii}(a_x,0) = T_{ii}(-a_x,0) = -0.72$ eV $\quad i = 1,\dots,4$ $T_{ii}(0,0) = 1.35$ eV
Intra-chain Ni-Ni hopping (a)-(b)	$T_{ii}(a_x,0) = T_{ii}(-a_x,0) = 0.30$ eV $\quad i = 5,6$ $T_{ii}(0,0) = -0.36$ eV
Intra-chain Ta-Ni hopping (c)-(d)	$T_{15}(\vec{0}) = -T_{15}(a_x,0) = T_{25}(\vec{0}) = -T_{25}(a_x,0) = 0.035$ eV $T_{36}(\vec{0}) = T_{46}(\vec{0}) = -T_{15}(\vec{0})$
Inter-chain Ta-Ni hopping (e)-(f)	$T_{45}(-a_x,a_y) = -T_{45}(a_x,a_y) = T_{35}(a_x,0) = -T_{35}(-a_x,0) = 0.04$ eV $T_{26}(a_x,0) = T_{16}(a_x,-a_y) = T_{45}(a_x,a_y)$
Inter-chain Ni-Ni hopping (g)	$T_{65}(a_x,a_y) = T_{65}(a_x,0) = T_{65}(0,0) = T_{65}(a_x,0) = 0.030$ eV
Inter-chain Ta-Ta hopping (h)-(i)	$T_{61}(-a_x,a_y) = T_{61}(0,a_y) = T_{23}(0,0) = T_{23}(a_x,0) = 0.020$ eV

Table I. Elements of the hopping matrix $\mathbf{T}(\vec{\delta})$. Matrix elements are grouped accordingly to the scheme in Fig. 2 with letters corresponding to the different hopping processes indicated by arrows.

and for $i \neq j$

$$\langle\Psi_0|\hat{n}_{j\sigma}(\vec{R})\hat{n}_{i\sigma'}(\vec{R}')|\Psi_0\rangle \approx \langle\Psi_0|\hat{n}_{j\sigma}(\vec{R})|\Psi_0\rangle\langle\Psi_0|\hat{n}_{i\sigma'}(\vec{R}')|\Psi_0\rangle - \delta_{\sigma\sigma'}\langle\Psi_0|c^\dagger_{j\sigma}(\vec{R})c_{i\sigma'}(\vec{R}')|\Psi_0\rangle\langle\Psi_0|c^\dagger_{i\sigma'}(\vec{R}')c_{j\sigma}(\vec{R})|\Psi_0\rangle. \quad (3)$$

Taking the variation with respect to $\langle\Psi_0|$ the HF Hamiltonian reads

$$\hat{H}_{HF} = \hat{H}_{hop} + \sum_{\mathbf{k}\sigma} \Psi^\dagger_{\mathbf{k}\sigma} \begin{pmatrix} \hat{h}_A(\mathbf{k}) & 0 \\ 0 & \hat{h}_B(\mathbf{k}) \end{pmatrix} \Psi_{\mathbf{k}\sigma} \quad (4)$$

where $\hat{h}_A(\mathbf{k})$ and $\hat{h}_B(\mathbf{k})$ are the decoupled interaction Hamiltonian for the A and B chain respectively. Specifically, accordingly to the atom labeling of Fig. 2,

$$\hat{h}_A(\mathbf{k}) = \begin{pmatrix} \delta\varepsilon_1 & 0 & w^*_{15}(\mathbf{k}) \\ 0 & \delta\varepsilon_2 & w^*_{25}(\mathbf{k}) \\ w_{15}(\mathbf{k}) & w_{25}(\mathbf{k}) & \delta\varepsilon_5 \end{pmatrix} \qquad \hat{h}_B(\mathbf{k}) = \begin{pmatrix} \delta\varepsilon_3 & 0 & w^*_{36}(\mathbf{k}) \\ 0 & \delta\varepsilon_4 & w^*_{46}(\mathbf{k}) \\ w_{46}(\mathbf{k}) & w_{46}(\mathbf{k}) & \delta\varepsilon_6 \end{pmatrix} \quad (5)$$

with

$$\delta\varepsilon_{i=1,2} = \frac{U}{2}n_i + 2Vn_5 \quad \delta\varepsilon_{i=3,4} = \frac{U}{2}n_i + 2Vn_6 \quad \delta\varepsilon_5 = \frac{U}{2}n_5 + 2V\left(n_1+n_2\right) \quad \delta\varepsilon_6 = \frac{U}{2}n_6 + 2V\left(n_3+n_4\right) \quad (6)$$

and

$$w_{i5} = -V\Delta_{i5}(\vec{0})(1-e^{-ik_xa}) - V\phi_{i5}e^{-ik_xa} \quad w_{i6} = -V\Delta_{i6}(\vec{0})(1-e^{ik_xa}) - V\phi_{i6}e^{ik_xa}. \quad (7)$$

In these equations $n_i = \langle\Psi_0|c^\dagger_{i\sigma}(\vec{0})c_{i\sigma}(\vec{0})|\Psi_0\rangle$, $\Delta_{ij}(\vec{0}) = \langle\Psi_0|c^\dagger_{i\sigma}(\vec{0})c_{j\sigma}(\vec{0})|\Psi_0\rangle$ and ϕ_{ij} are the order parameters defined in the main text. All the above parameters are self-consistently determined by diagonalizing the HF Hamiltonian starting from an initial guess.

B. Double Counting Corrections

To avoid double counting of correlation effects within our Hartree-Fock calculations which are already present on the level of the DFT calculations, we make use of cRPA Coulomb matrix elements and apply a double counting correction potential to the bare band structure. The former aims to avoid a double counting of screening processes to the Coulomb interactions resulting from the model band structure. By excluding these screening processes in cRPA calculations for the Coulomb matrix elements based on the full ab initio band structure we take screening from the "rest" of the band structure into account, but not from the bands of the minimal model. A double counting of this kind is thus avoided in the interaction terms. On the other side, the double-counting potential is introduced to not count twice the effect of local interactions already included in DFT. The commonly used ansatz for this is an orbital-independent potential which is acting only on the correlated orbitals. Since our minimal model is completely down-folded to correlated orbitals only, a potential of this form would equally shift all involved bands and would thus have no effect at all. We can thus safely neglect a double-counting correction potential of this form.
Care must, however, be taken due to the use of the modified Becke-Johnson (mbj) exchange potential (in contrast to GGA or LDA approximations). Although this exchange potential is still local, it effectively accounts for non-local Coulomb interaction terms here. The most prominent effect of the mbj exchange potential for Ta_2NiSe_5 is to decrease the overlap between the mostly Ta-like conduction bands with the mostly Ni-like valence bands, which is controlled by the mbj parameter c_{mbj}. For $c_{\mathrm{mbj}} = 1.0$ the results are very similar to GGA/LDA calculations with a an overlap of about 400 meV at Z. For our self-consistently calculated $c_{\mathrm{mbj}} = 1.26$ the overlap is approx. 200 meV. In order to not double-count this decreasing trend of the overlap upon inclusion of correlation effects, the Ta and Ni onsite energies of our minimal model are adjusted to result in an overlap of about 400 meV (see Fig. 2 B). We also checked the influence of this procedure and find that all of our conclusions hold independently on the exact value of this change in the overlap. The phase diagram looks qualitatively the same and just slight quantitative changes are observed so that the critical values $V_l^*(U)$ and $V_u^*(U)$ shift to slightly larger values upon increasing the band overlap in the bare minimal model.

---

* These two authors equally contributed
giacomo.mazza@unige.ch
m.roesner@science.ru.nl
† ageorges@flatironinstitute.org

[1] John P. Perdew, Kieron Burke, and Matthias Ernzerhof. Generalized Gradient Approximation Made Simple. *Physical Review Letters*, 77(18):3865–3868, October 1996.
[2] P. E. Blöchl. Projector augmented-wave method. *Physical Review B*, 50(24):17953–17979, December 1994.
[3] G. Kresse and J. Furthmüller. Efficiency of ab-initio total energy calculations for metals and semiconductors using a plane-wave basis set. *Computational Materials Science*, 6(1):15–50, July 1996.
[4] G. Kresse and J. Furthmüller. Efficient iterative schemes for ab initio total-energy calculations using a plane-wave basis set. *Physical Review B*, 54(16):11169–11186, October 1996.
[5] Steven A. Sunshine and James A. Ibers. Structure and physical properties of the new layered ternary chalcogenides tantalum nickel sulfide (ta2nis5) and tantalum nickel selenide (ta2nise5). *Inorganic Chemistry*, 24(22):3611–3614, 1985.
[6] Axel D. Becke and Erin R. Johnson. A simple effective potential for exchange. *The Journal of Chemical Physics*, 124(22):221101, 2006.
[7] Fabien Tran and Peter Blaha. Accurate Band Gaps of Semiconductors and Insulators with a Semilocal Exchange-Correlation Potential. *Phys. Rev. Lett.*, 102:226401, Jun 2009.
[8] Arash A. Mostofi, Jonathan R. Yates, Young-Su Lee, Ivo Souza, David Vanderbilt, and Nicola Marzari. wannier90: A tool for obtaining maximally-localised Wannier functions. *Computer Physics Communications*, 178(9):685–699, May 2008.
[9] F. Aryasetiawan, M. Imada, A. Georges, G. Kotliar, S. Biermann, and A. I. Lichtenstein. Frequency-dependent local interactions and low-energy effective models from electronic structure calculations. *Phys. Rev. B*, 70:195104, Nov 2004.
[10] Merzuk Kaltak. *Merging GW with DMFT*. Phd thesis, University of Vienna, 2015.
[11] Ersoy Sasioglu, Christoph Friedrich, and Stefan Blügel. Effective coulomb interaction in transition metals from constrained random-phase approximation. *Phys. Rev. B*, 83:121101, Mar 2011.